Supplementary Information

Self- Assembling CuS Anodes with Conversion Reaction for Ultrafast Na-ion Storage

Sung Yeob Kim[1,†], Hee-Jae Ahn[1,†], Young-Hoon Kim[1], Hong-Kyu Kim[2], Byeong-Hyeon Lee[2], Young-Woon Byeon[3], Jae-Ho Park[4], Kyung Yoon Chung[4,5], Jae-Chul Lee[1,6]*

[1]Department of Materials Science and Engineering, Korea University, Seoul 02841, South Korea

[2]Advanced Analysis Center, Korea Institute of Science and Technology, Seoul 02792, South Korea

[3]Materials Sciences Division, Lawrence Berkeley National Laboratory, Berkeley, CA 94720, USA

[4]Energy Storage Research Center, Korea Institute of Science and Technology, Seoul 02792, South Korea

[5]Division of Energy & Environment Technology, Korea University of Science and Technology, Seoul 02792, South Korea

[6]Institute of Green Manufacturing Technology, Korea University, Seoul 02841, South Korea

Methods

Preparation of the anodes. To prepare the CuS electrode for the Na–CuS half-cells, polyacrylic acid (PAA, average M_v of ca. 450,000, Sigma-Aldrich) was first dissolved in a deionized water. The commercial CuS particles (hexagonal, −100 mesh, Sigma-Aldrich) and conductive additive of multi-walled carbon nanotubes (MWCNT, AM90, ACN Co.) were then mixed with the PAA solution at a weight ratio of 80:10:10 using a planetary ball mill (Pulverizette 7, Fritsch GmbH) for 3 h at 300 rpm. For a comparative study, Sn and Pb electrodes were also prepared using commercial Sn (tetragonal, −100 mesh, Sigma-Aldrich) and Pb (cubic, −325 mesh, Sigma-Aldrich) particles and the same procedures. The slurry mixtures were coated on the Cu current collector and dried at 80 ℃ in vacuum for 24 h. The mass loading of the active materials on the dried electrodes was 1.2 mg cm^{-2} for Sn, Pb, and CuS anodes.

Preparation of the half-cells. The CuS working electrode and Na metal counterpart/reference electrode were assembled in an air-tight Ar-filled globe box to fabricate Swagelok-type cells. A polypropylene nano-porous membrane (25 μm, Celgard 2400) and glass-fibre filter (670 μm, GF/D, WhatmanTM) were used as CuS- and Na-side separator membranes, respectively. 1 M $NaPF_6$ (98%, Sigma-Aldrich) in DME (99.5%, Sigma-Aldrich) was used as the liquid electrolyte. To analyse the effects of the different electrolytes on the coalescence reaction between CuS nanoparticles, counterpart cells with different solvent types were assembled using 1 M of NaPF6 dissolved in a 1:1 vol% mixture of EC (99.5%, Sigma-Aldrich) and DEC (99.5%, Sigma-Aldrich) solvents. For a comparative study, Na–Sn and Na–Pb half-cells were also prepared using the same procedures.

Electrochemical tests. The charge(desodiation)/discharge(sodiation) tests were performed using a galvanostat (WBCS 3000, WonA Tech Co.) in a constant-current mode by varying the

potential in the range of 0.01–3.0 V for Na–CuS half-cells and 0.001–1.0 V for Na–Sn and Na–Pb half-cells at 24 °C. All measurements were performed after running the first cycle at 0.1C for electrical stabilization. Electrochemical cycling tests were performed at the charging rates of 0.1–100C for Na–Sn (1C = 847 mAg^{-1}), Na–Pb (1C = 485 mAg^{-1}), and Na–CuS (1C = 560 mAg^{-1}) systems. The impedance spectra (or Nyquist plots) were measured using electrochemical impedance spectroscopy (EIS, VSP-300, Bio-logic) in the frequency range of 7 MHz to 100 mHz at 30 mV and at 25°C.

Material characterization. The crystal structures of bulk CuS, Sn, and Pb were confirmed by X-ray diffraction (XRD, MAX-2500V, Rigaku). X-ray photoelectron spectroscopy (XPS, X-TOOL, ULVAC-PHI) was conducted to confirm the oxidation state of CuS particles. Scanning electron microscopy (SEM, S-4800, Hitachi) was employed to trace the morphological evolution sequence of bulk Sn, Pb, and CuS particles associated with battery cycling.

Cross-sectional milling and chemical analyses. To identify the composition of the anodes subjected to sodiation, the cross-sections of Sn, Pb, and CuS anodes were prepared from the respective cells subjected to sodiation at 30C using an Ar ion milling machine (Hitachi High-Tech Inc., ArBlade 5000) at an operating voltage of 4 kV, a milling angle of 40˚, a swing rate of 5 rpm, and a milling time of 2 h. The samples were then transferred to an SEM device using a vacuum holder to prevent contamination by air and moisture. The compositions were measured for all possible elements (Na, Sn, Pb, Cu, S, P, F, C, and O) comprising the samples using energy dispersive X-ray spectroscopy (EDS, Oxford, ULTIM MAX 170). The electric current applied by SEM and EDS was controlled to be lower than usual (5 keV and 37 pA for SEM and 5 keV, 3.9 nA for EDS) to minimize electron beam damage on the target materials.

Structure analyses. Prior to sample preparation, the surface of the fully sodiated CuS anode was coated with epoxy to avoid Ga-ion implantation or possible sample damage. The target

region was milled with a Ga ion beam at 30 kV to prepare a few-μm-thick section. The prepared section was picked up from the bulk specimen and fixed onto a Mo grid for further thinning. The fixed specimen was milled with a Ga ion beam at 5 kV to prepare a thin section of a thickness < 100 nm. The sample was then transferred to a transmission electron microscopy (TEM, TECNAI, Thermofisher) device using an airtight sample transfer device to observe the microstructures and selected area electron diffraction patterns at 200 kV.

Diffusivity measurement of the intermediate phases. The galvanostatic intermittent titration technique (GITT) tests were performed using a galvanostat (WBCS 3000, WonA Tech Co.). The cell was discharged with a current impulse with the current density of 0.1C for an interval (τ) of 600 s followed by a rest process for 3600 s without a current impulse. The Na diffusivities (^{D_i}) of the intermediate phases (i) in the Sn, Pb, and CuS anodes were determined using GITT data according to equation (1):

$$D_i = \frac{4}{\pi\tau}\left(\frac{mV}{MA}\right)^2\left(\frac{\Delta E_s}{\Delta E_\tau}\right)^2 \quad \left(\tau \ll \frac{L^2}{D}\right), \tag{1}$$

where m, M, V, A, and L are the active material mass in the electrode, molecular weight of Sn, Pb, and CuS, molar volume of Sn, Pb, and CuS, electrode surface area, and thickness of the electrode. ΔE_s is the change of the steady-state potential after a discharge pulse and rest process, while ΔE_τ is the voltage change during a discharge pulse.

Interfacial interaction calculations. We used the Quantum Espresso software package[1] with norm-conserving pseudopotentials[2] to calculate the interactions between CuS nanoparticles (NPs) and three solvent molecules (EC, DEC, and DME). Prior to simulating the NP surface interactions, CuS slabs and the three solvent molecules were modeled. During sodiation in Na-CuS systems, Na is inserted in the <010> direction (with respect to CuS)[3]. Furthermore, solvent

molecules within the electrolyte tend to react with the (010) surface of CuS due to its high surface energy (Figure S22). Therefore, we evaluated the interaction between the CuS slab (010) surface and the solvent molecules (EC, DEC, and DME). To prevent the periodic image of the CuS slab, an additional vacuum layer was added to the free-surface side of the CuS slab for each model structure. The geometry of the CuS NP/electrolyte interfaces was optimized in the canonical (NVT) ensemble using a conjugate-gradient algorithm. The CuS slab was set to a positively charged (+3) state to replicate the positively charged CuS NPs. A plane-wave expansion cut-off energy of 30 Ry and Monkhorst–pack scheme with a k-point mesh of 2 × 2 × 1 were used for Brillouin zone sampling. Energy convergence was achieved down to 0.2 Ry/unit cell.

Adsorption energy calculations. The adhesion tendencies of EC, DEC, and DME solvents to the CuS NP were quantitatively determined by calculating their adsorption energies. To do so, we first optimized the geometries of the CuS NP/electrolyte interface, CuS slab, and individual molecules comprising the electrolytes and calculated their total energies. The adsorption energies (ΔE_{ads}) of the individual solvent molecules were then determined using the following equation:

$$\Delta E_{ads} = E_{(slab + molecule)} - E_{slab} - \Delta E_{molecule}, \qquad (2)$$

where E_{slab}, $E_{molecule}$, and $E_{(slab\ +\ molecule)}$ represent the DFT total energies of the CuS slab, individual solute ion or solvent molecule, and adsorbed molecule on the CuS slab, respectively. A negative E value, denoting an exothermic process, signifies a stable adsorption.

Resistivity calculations of the intermediate phases. The electrical resistivities of 14 phases formed in the Na–Sn, Na–Pb, and Na–CuS systems were evaluated by identifying their electronic structures using DFT calculations with a plane-wave basis set and norm-conserving

pseudopotentials[2], as implemented in Quantum Espresso[1]. The plane-wave cutoff energy was set to 50 Ry, and energy convergence was achieved at 0.2 Ry per unit cell. Brillouin zone sampling was performed using the Monkhorst–Pack scheme with a k-point mesh set to 8 × 8 × 8. The computed electronic structures were converted to electrical resistivity values using the Boltzmann transport theory, as implemented in the Boltzmann Transport Properties (BoltzTraP) code[4].

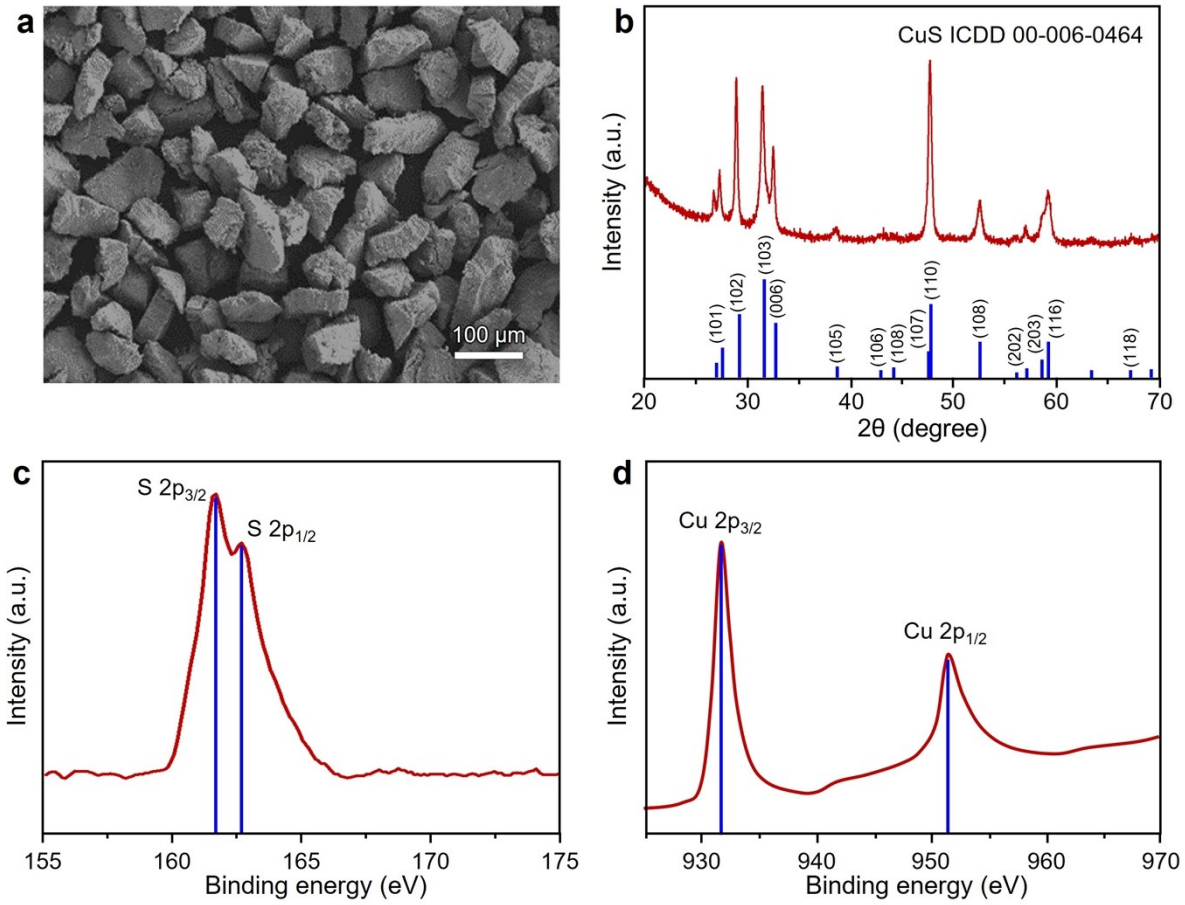

Figure S1. (a) Secondary electron image of the commercial micro-sized CuS powders, showing the morphologies of CuS particles. PXRD pattern of (b) CuS and XPS spectra of (c) Sulfur and (d) Copper recorded from the CuS particles. The peaks obtained from XRD are well matched to the hexagonal structure of CuS, whereas the XPS peaks at 162.6, 161.5, 931.6 and 951.6 eV correspond to the binding energies of S $2P_{3/2}$, S $2P_{1/2}$, Cu $2P_{3/2}$ and Cu $2P_{1/2}$, respectively. The S 2p XPS data clearly confirms the presence of S–S linkages in CuS (hexagonal). This phenomenon is primarily attributed to the existence of S–S bonds along the <001> direction (c-axis) on the surface of hexagonal CuS[5]. Additionally, the formation of S–S bonds is facilitated by the considerably lower formation energy of Cu vacancies within the (001) surface of CuS compared to the formation energy of S vacancies[6].

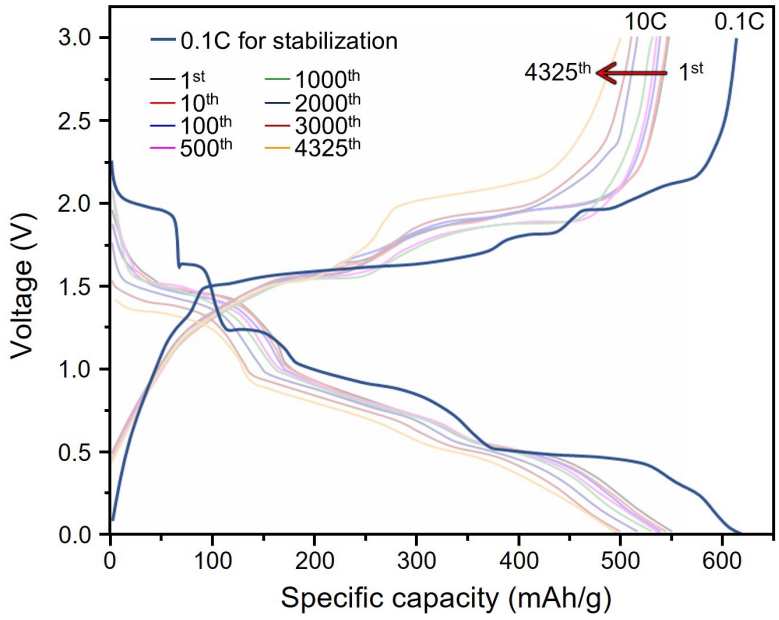

Figure S2. Variations in the capacity of the Na–CuS half-cell with DME solvent measured as a function of the cycle. Cell tests were performed at 10C after running the first cycle at 0.1C for electrical stabilization.

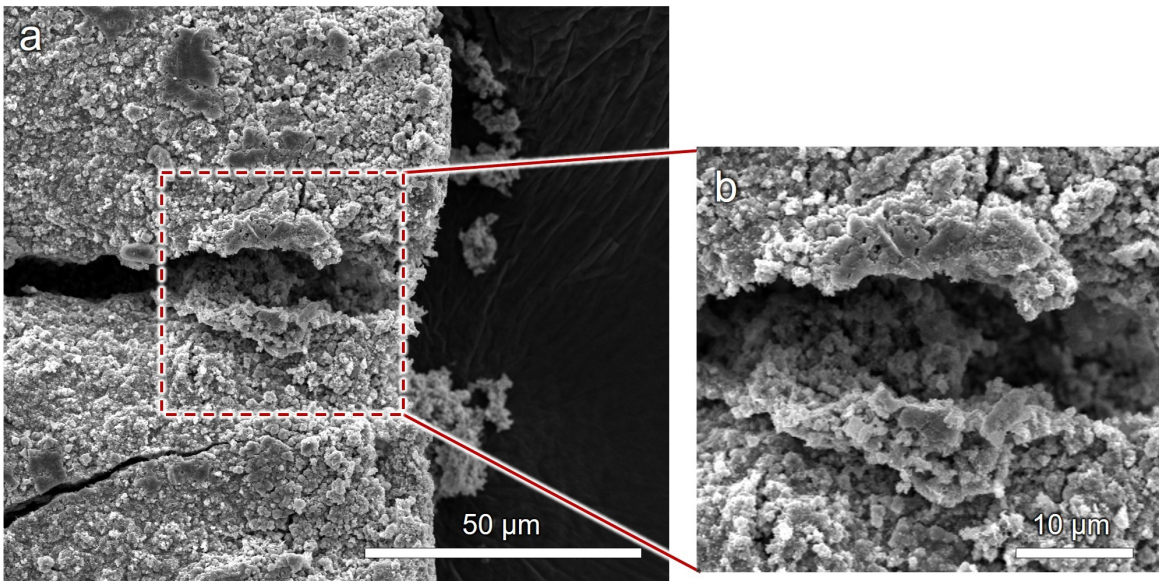

Figure S3. (a) Secondary electron image of the CuS particle extracted from the 50-times-cycled Na–CuS half-cell with an electrolyte comprising 1M $NaPF_6$ dissolved in EC/DEC solvent. (b) Magnified image of the region outlined by the rectangle in (a), showing the eroded surface by the fragmentation of CuS particles.

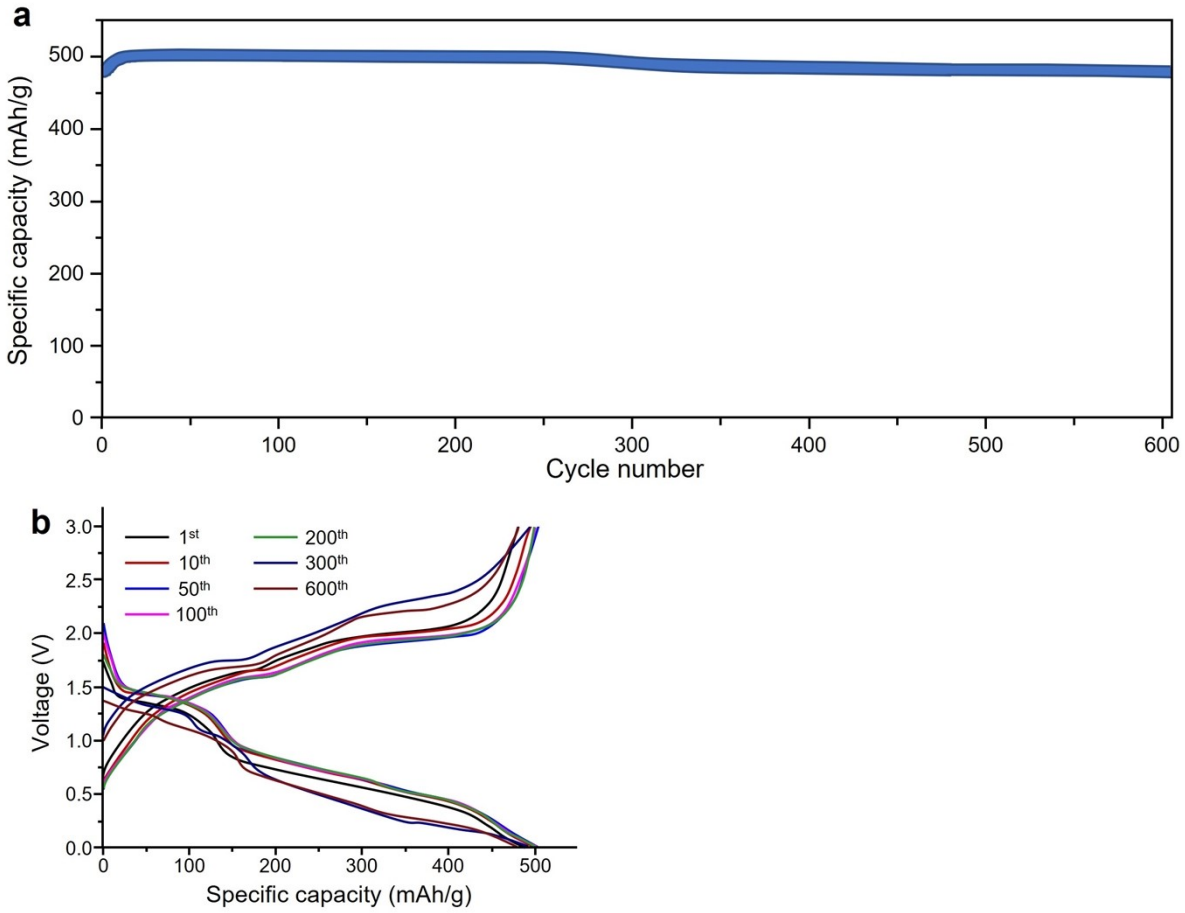

Figure S4. (a) Variations in the specific capacity and (b) voltage-capacity profiles of the Na–CuS half-cell with the DME solvent measured at 30C (16.8 A/g) for 1000 cycles, showing a superior cycling stability and reversibility of the CuS anode. Note that the specific capacity was measured after running the first cycle at 0.1C for electrical stabilization.

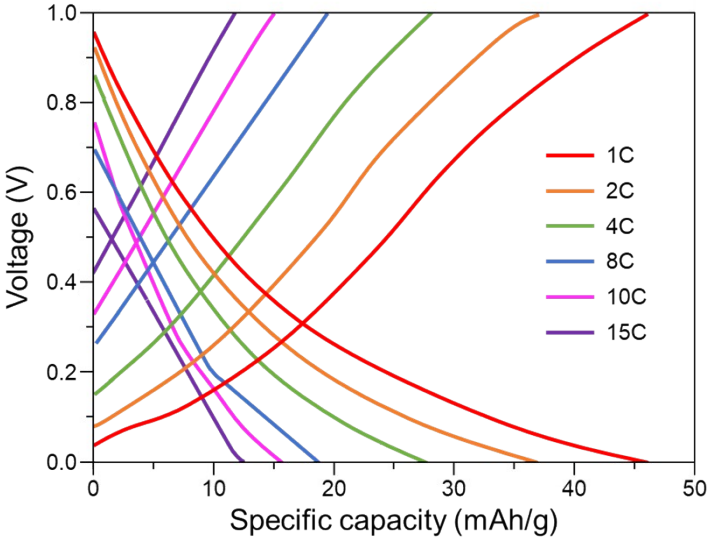

Figure S5: Discharge/charge voltage profiles of the MWCNTs measured at various current rates.

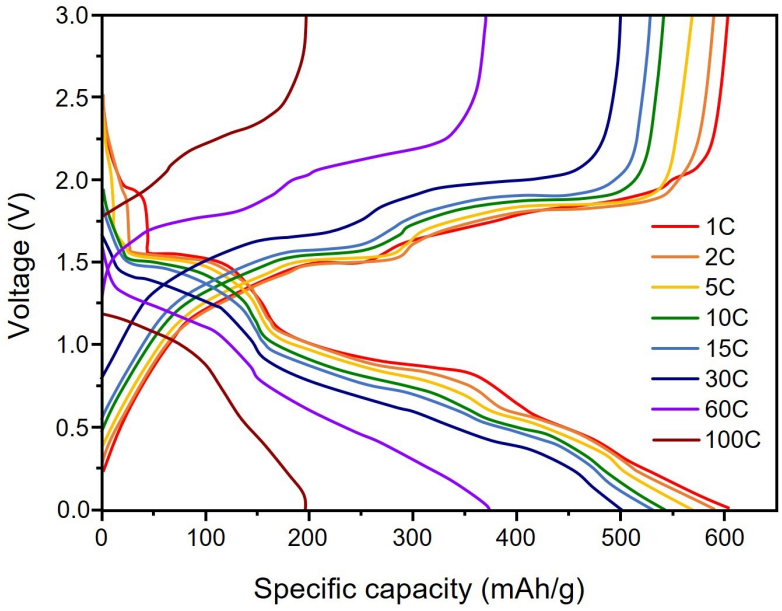

Figure S6. Changes in the voltage-capacity profiles measured at various C-rates for the Na–CuS half-cells with an electrolyte containing DME.

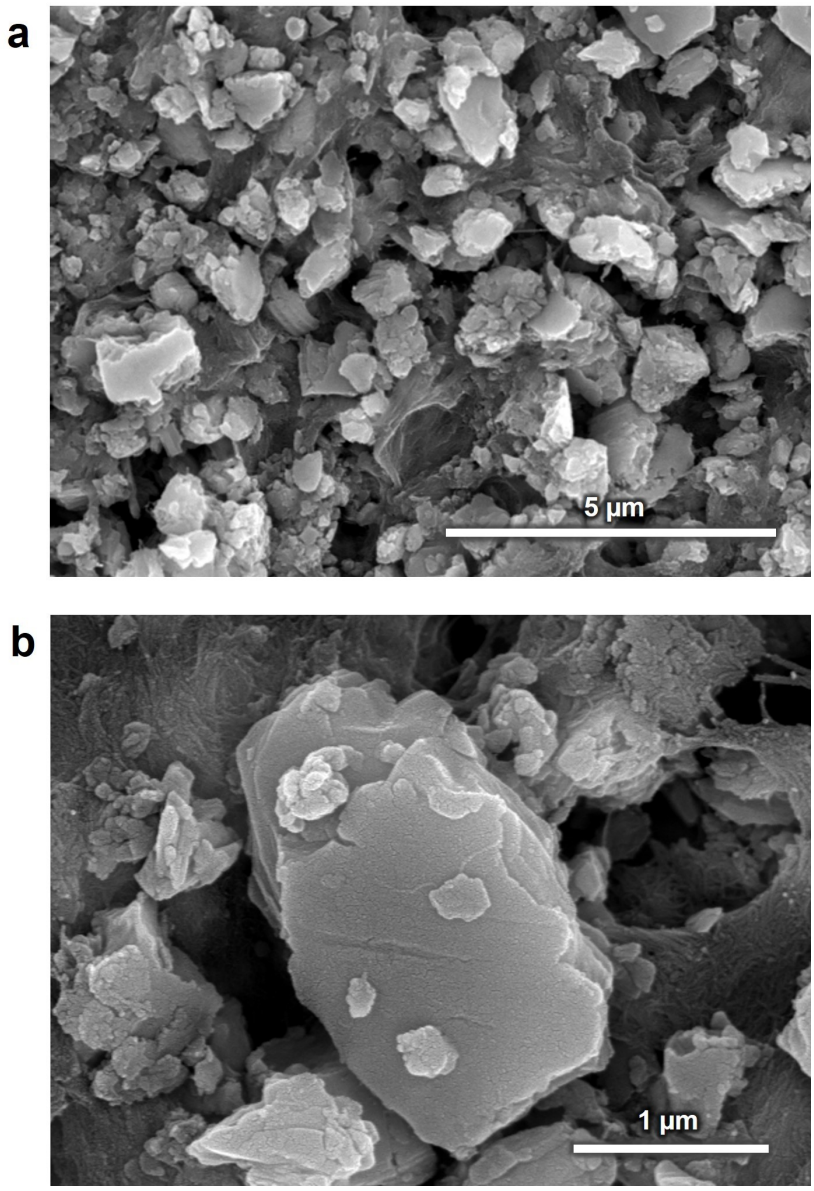

Figure S7. Secondary electron images recorded at (a) low and (b) high magnifications from the uncycled CuS anode, showing the surfaces of the CuS particles.

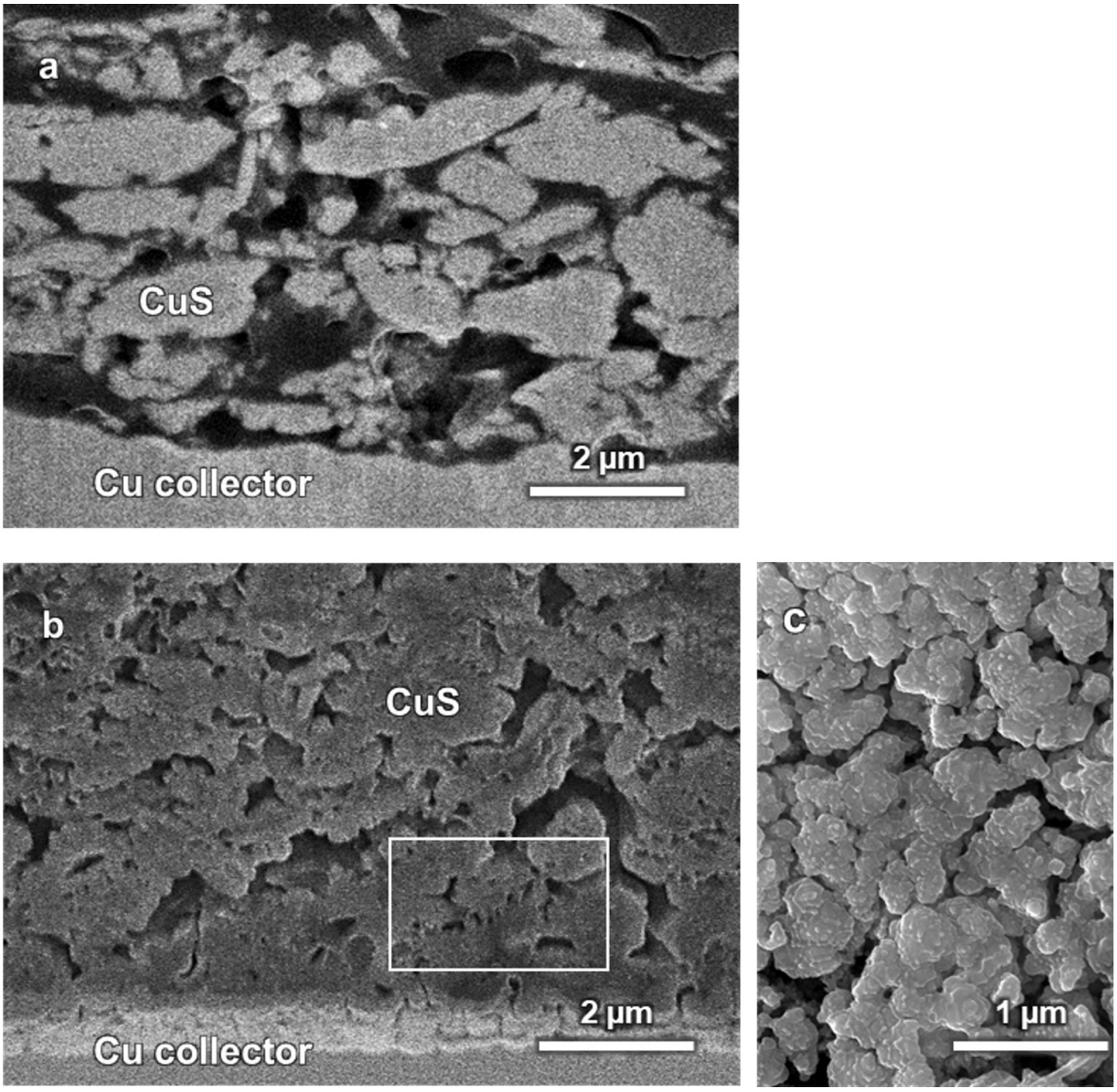

Figure S8. Secondary electron images of the cross sections prepared using FIB for the (a) uncycled and (b) 50-times-cycled CuS anode. (c) Magnified image recorded from the region similar to the rectangle denoted in (b), showing that separate CuS particles started to agglomerate after 50 cycles to form a loosely connected microscale structure. Note that all images were obtained from the cross sections of the CuS anodes along the thickness direction. The structure shown in (b) eventually transforms to a porous nanostructure with further cycling.

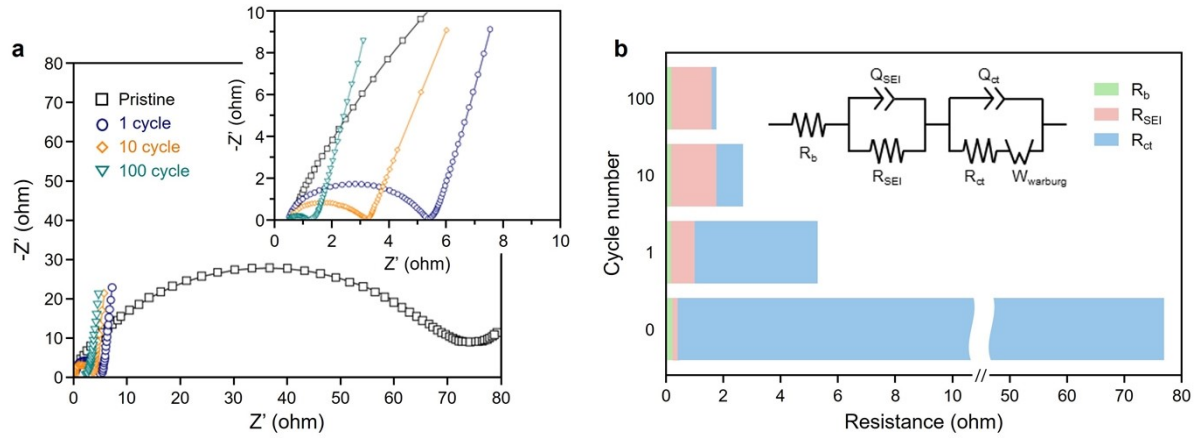

Figure S9. (a) Nyquist plots of the Na–CuS half-cells with the electrolyte containing DME solvents at various cycles. (b) Values of bulk resistance (R_b), SEI resistance (R_{SEI}), and charge transfer resistance (R_{ct}) deconvoluted from based on the Nyquist plots in Figure S9(a). An equivalent circuit model depicted in the inset was used for fitting, where "Q" means a constant phase element and "W" means Warburg resistance. EIS measurements were performed at 1C.

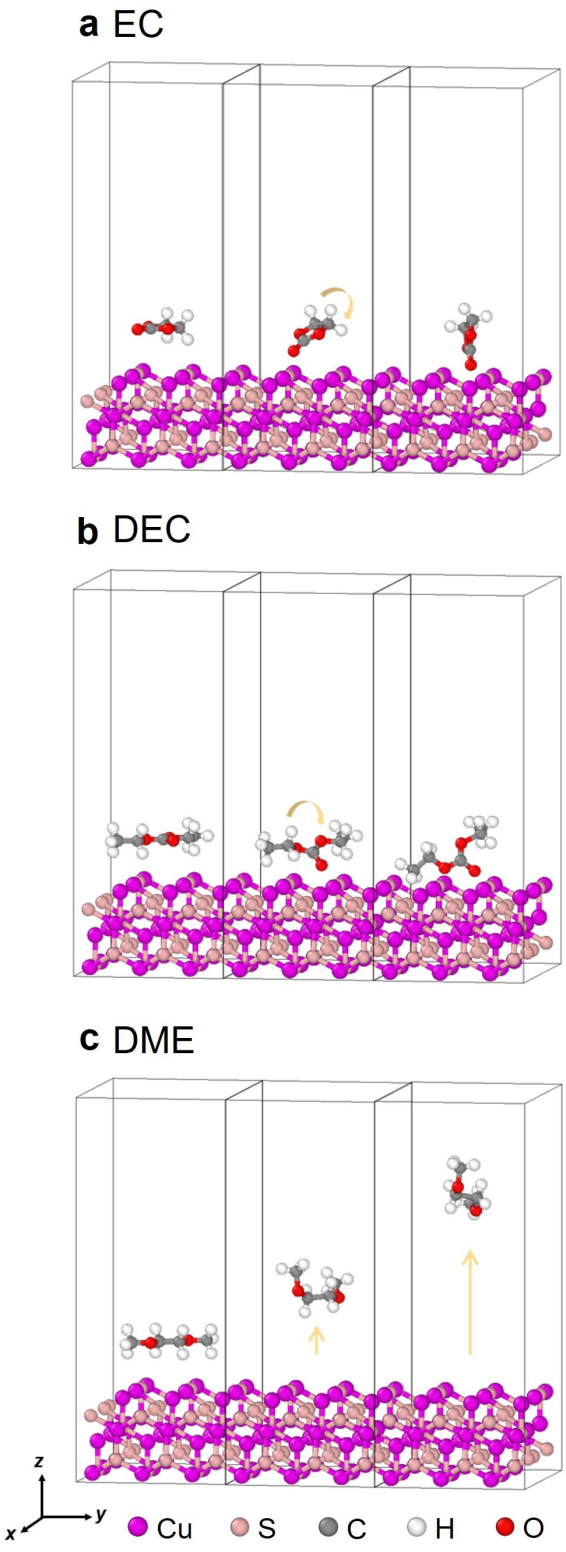

Figure S10. Optimized structures of the CuS/electrolyte interfaces obtained from DFT calculations, revealing the interactions between CuS and the electrolyte components: (a) EC, (b) DEC, and (c) DME. It is noteworthy that the molecular EC and DEC rotate so that their negatively charged ends are adsorbed to the CuS surface.

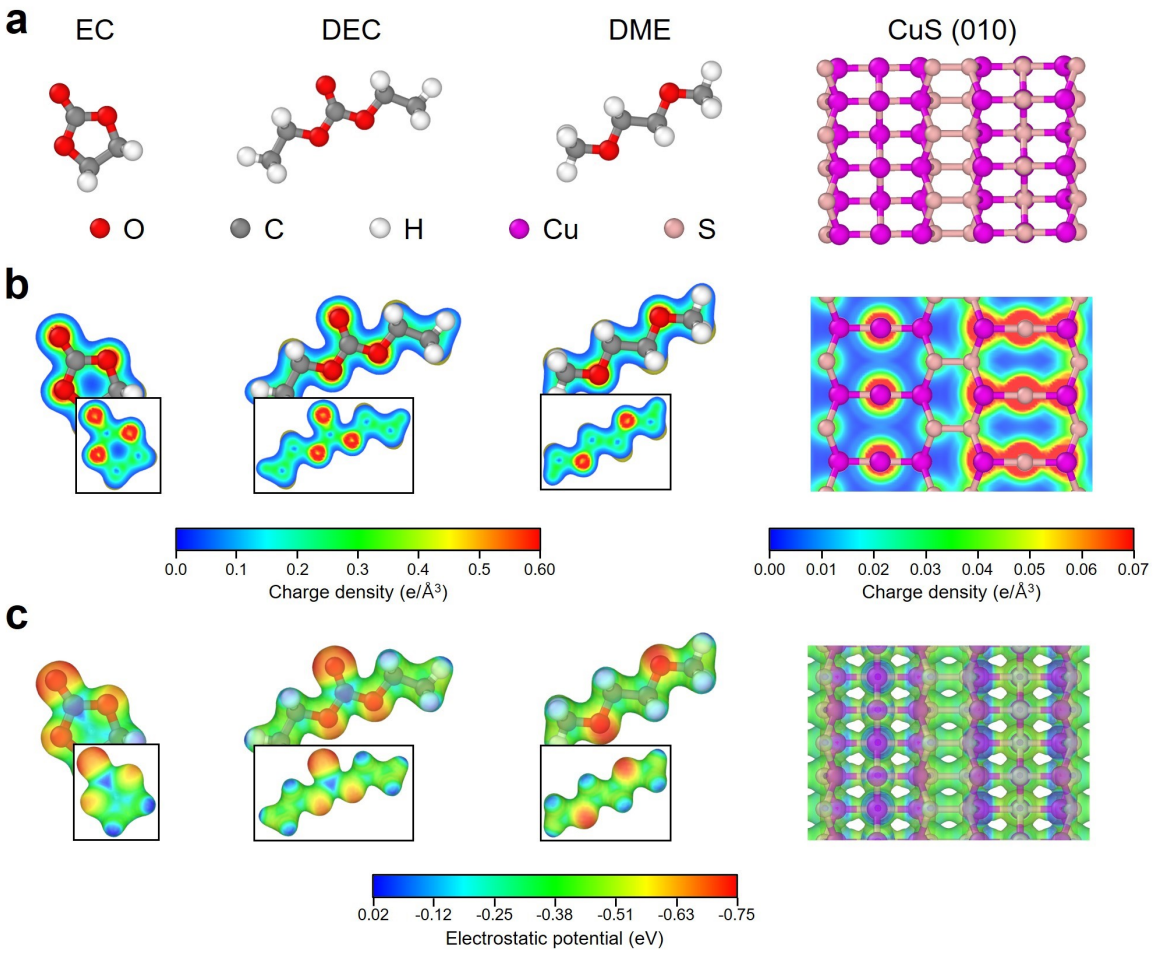

Figure S11. (a) Atomic configurations and (b) charge density distributions and (c) electrostatic potential of solvent molecules (EC, DEC, and DME) and active material (CuS) optimized using DFT calculations.

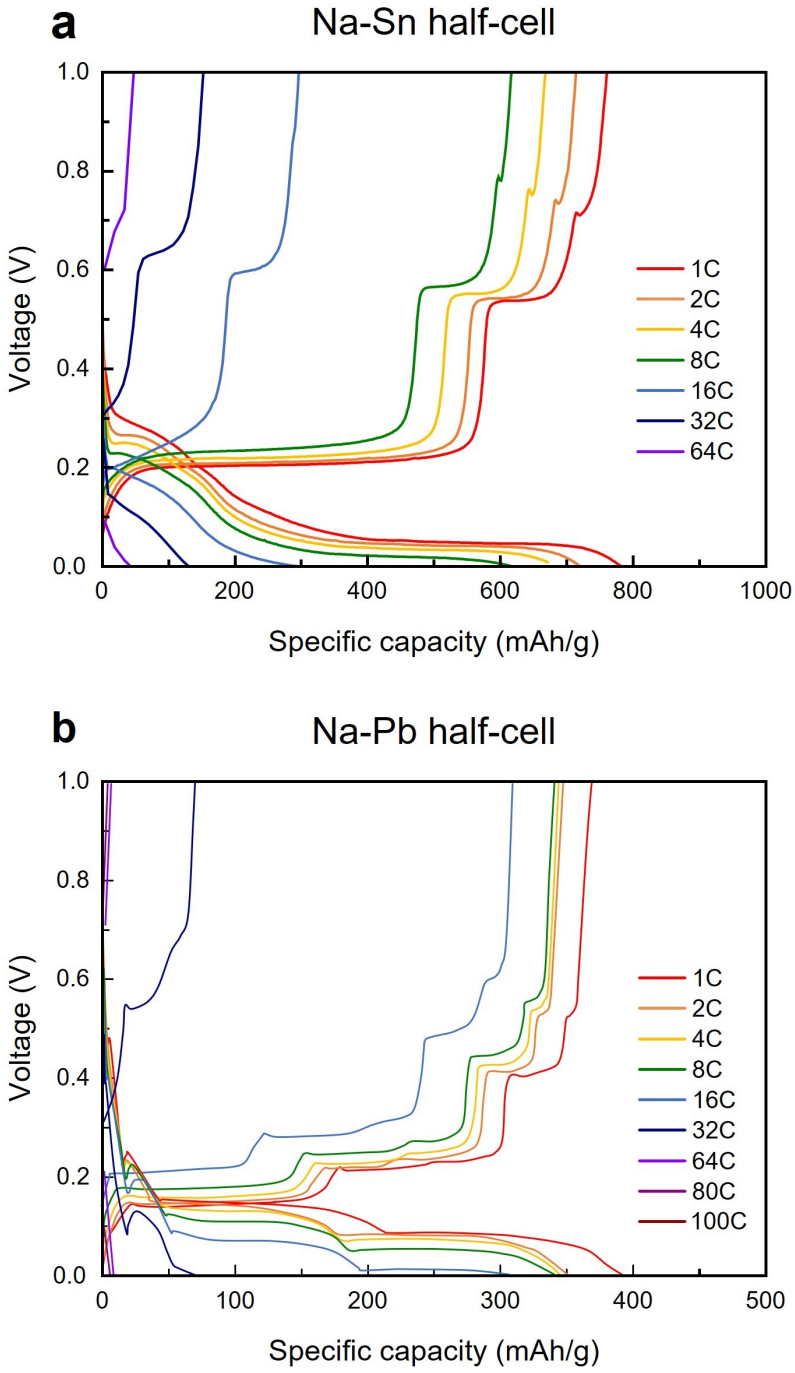

Figure S12. Changes in the voltage-capacity profiles measured at various C-rates for the (a) Na–Sn and (b) Na–Pb with an electrolyte containing DME.

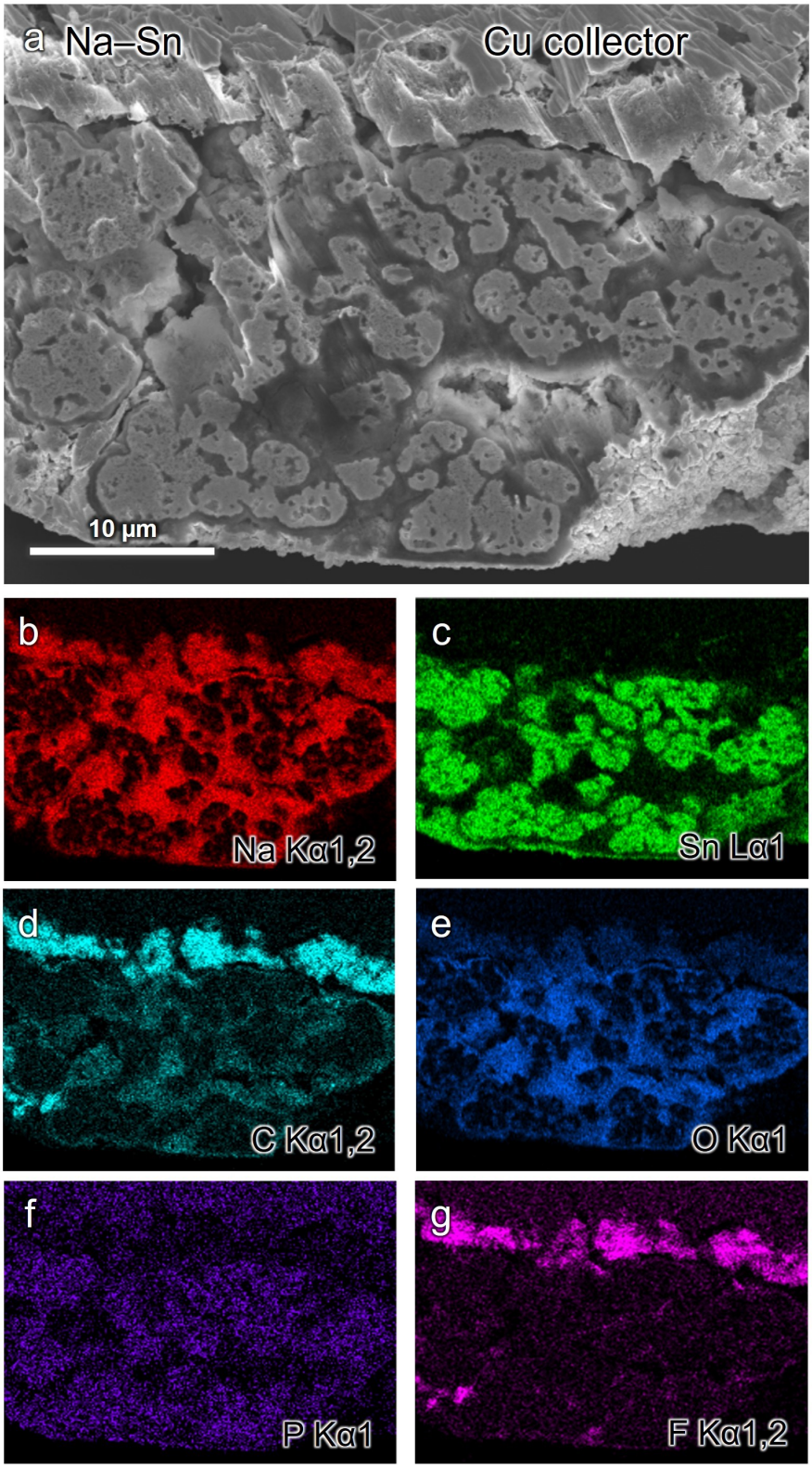

Figure S13. (a) Secondary electron images and (b-g) EDS elemental maps recorded from the cross-section of the Sn anode subjected to sodiation at 30C.

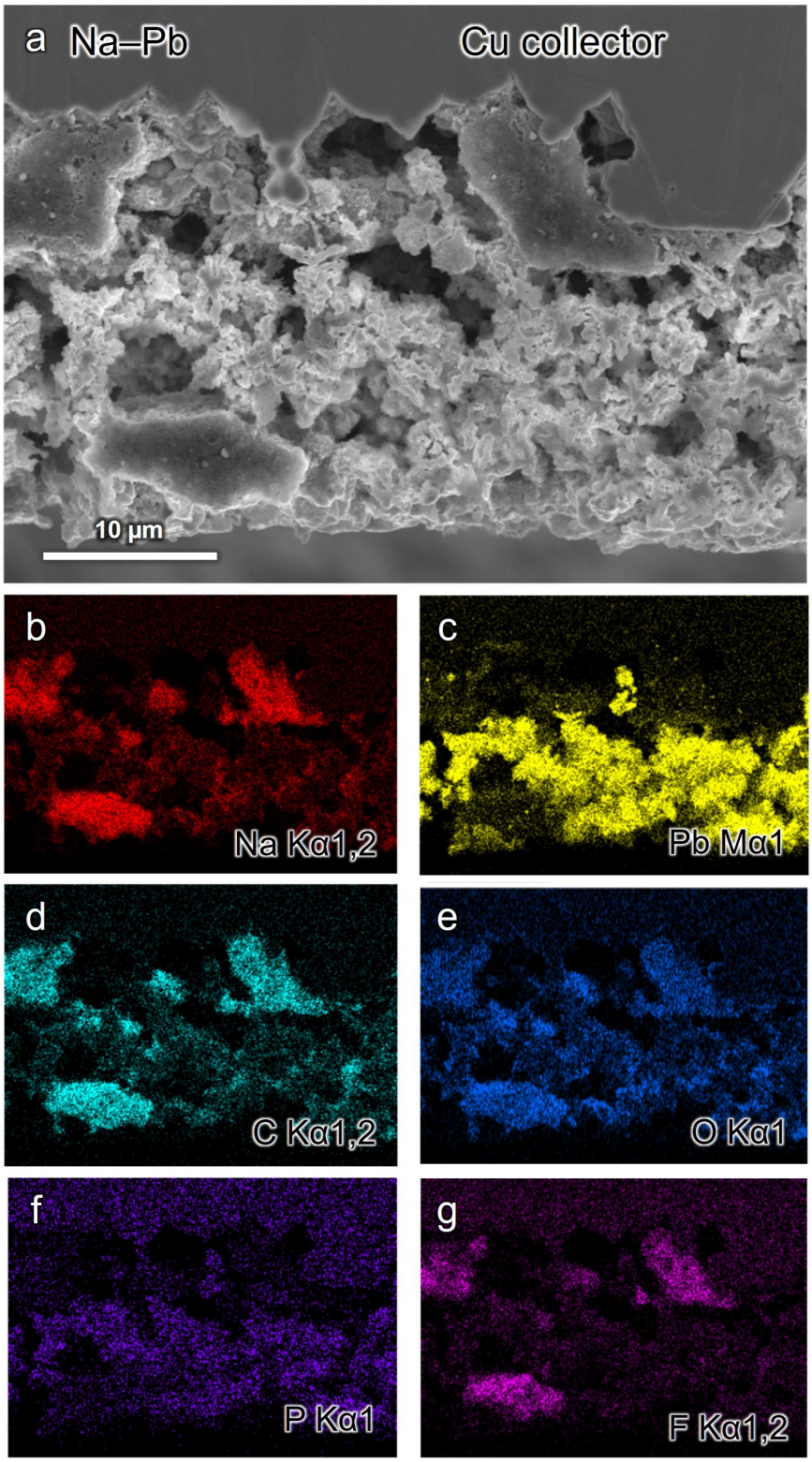

Figure S14. (a) Secondary electron images and (b-g) EDS elemental maps recorded from the cross-section of the Pb anode subjected to sodiation at 30C.

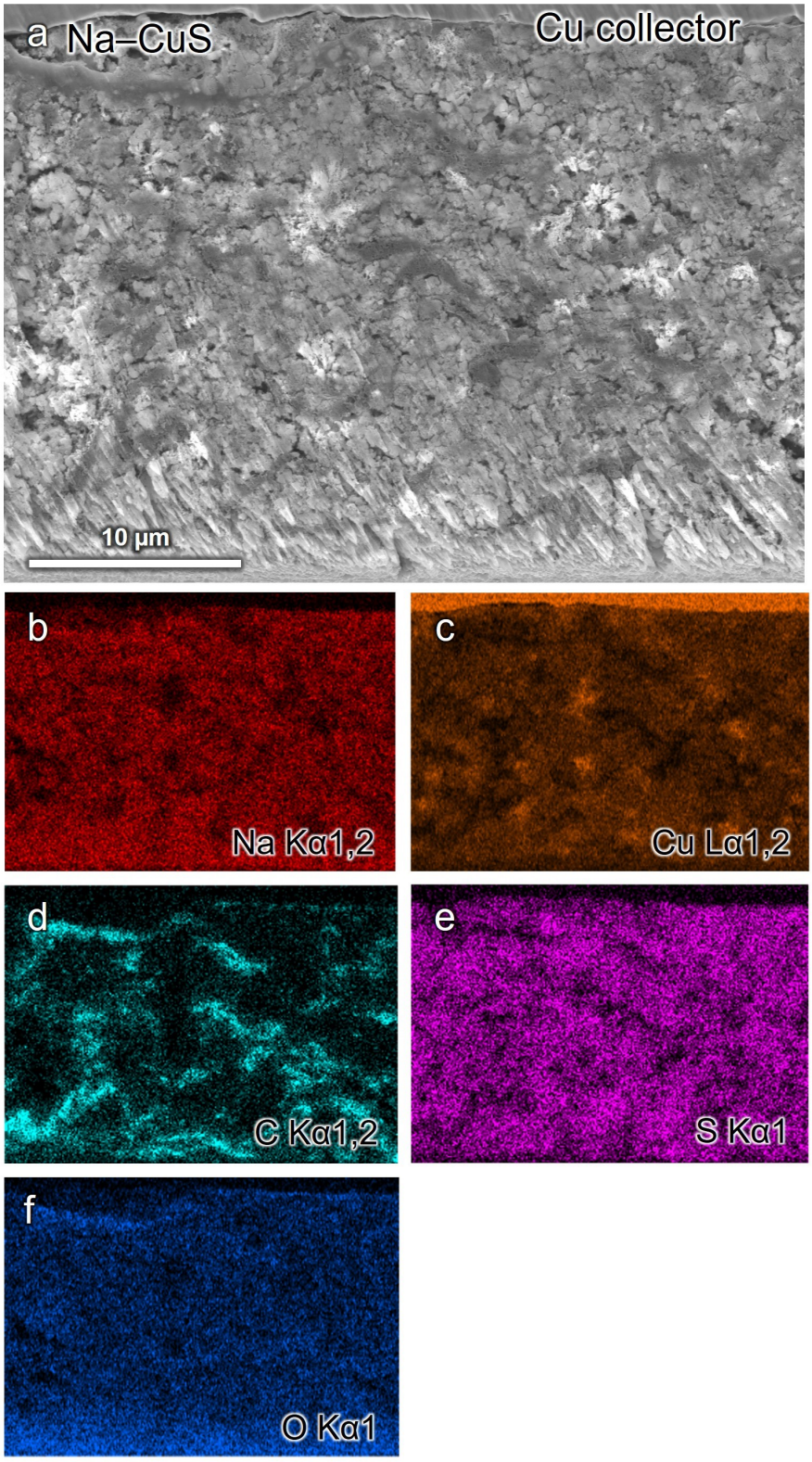

Figure S15. (a) Secondary electron images and (b-f) EDS elemental maps recorded from the cross-section of the CuS anode subjected to sodiation at 30C.

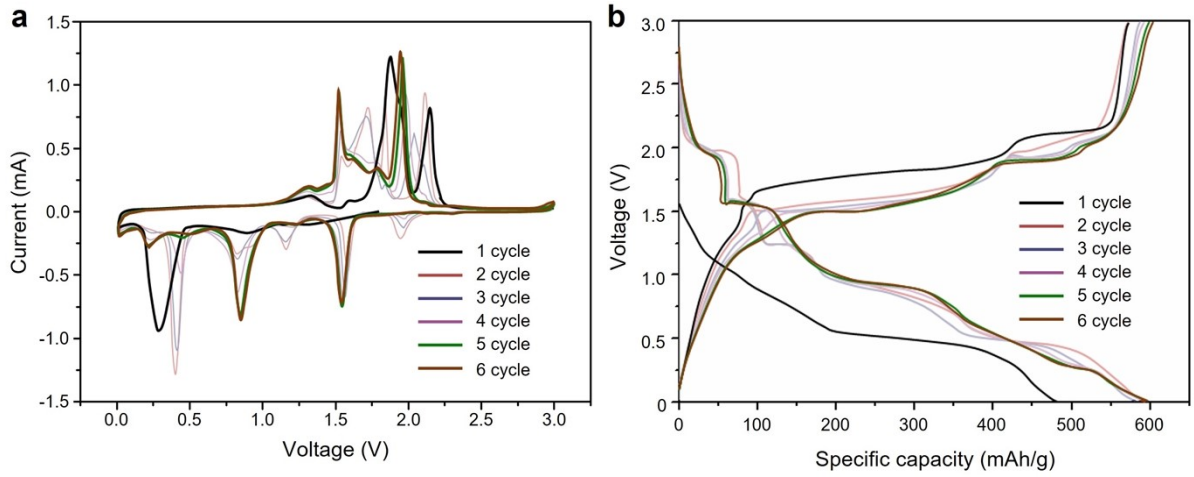

Figure S16. (a) Cyclic voltammetry curves of CuS anodes measured at various scan rates and (b) discharge/charge voltage profiles of Na–CuS half-cell with DME solvent measured at 0.1C (56 mA/g).

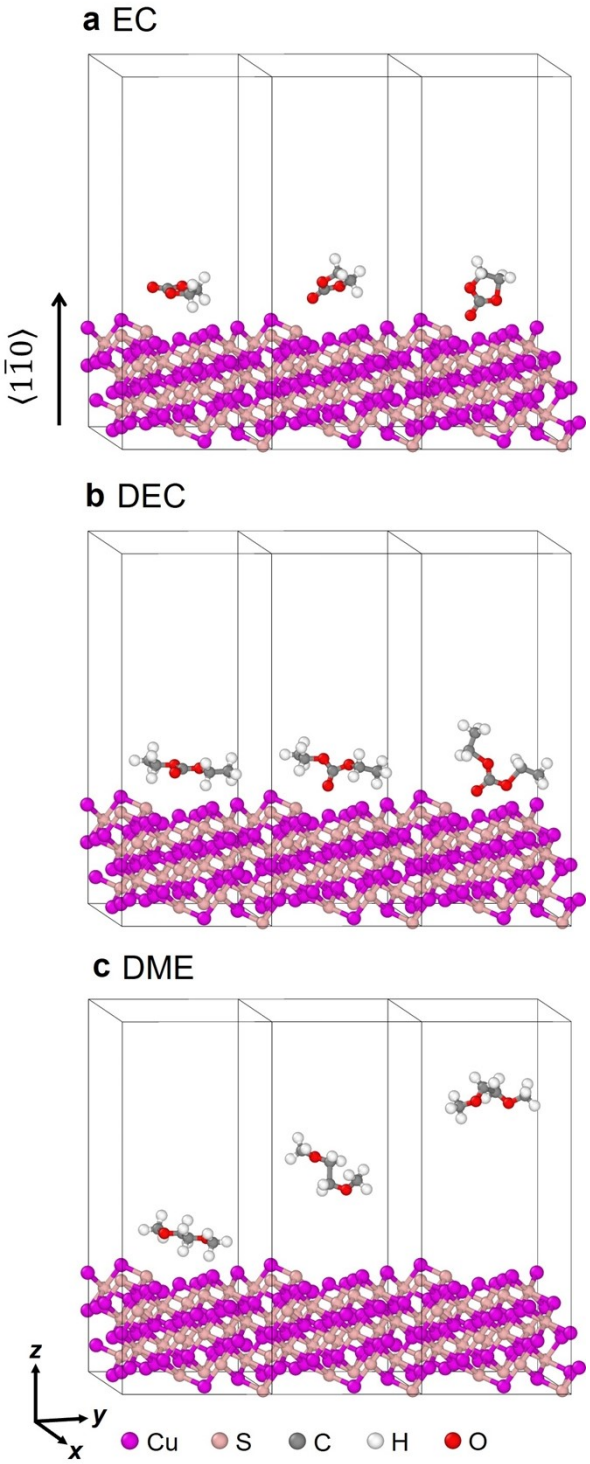

Figure S17. Optimized structures between the $Cu_{1.81}S$ ($1\bar{1}0$) surface and electrolyte obtained from DFT calculations, revealing the interactions between $Cu_{1.81}S$ and the electrolyte components: (a) EC, (b) DEC, and (c) DME. It is noteworthy that the molecular EC and DEC rotate so that their negatively charged ends are adsorbed to the $Cu_{1.81}S$ ($1\bar{1}0$) surface.

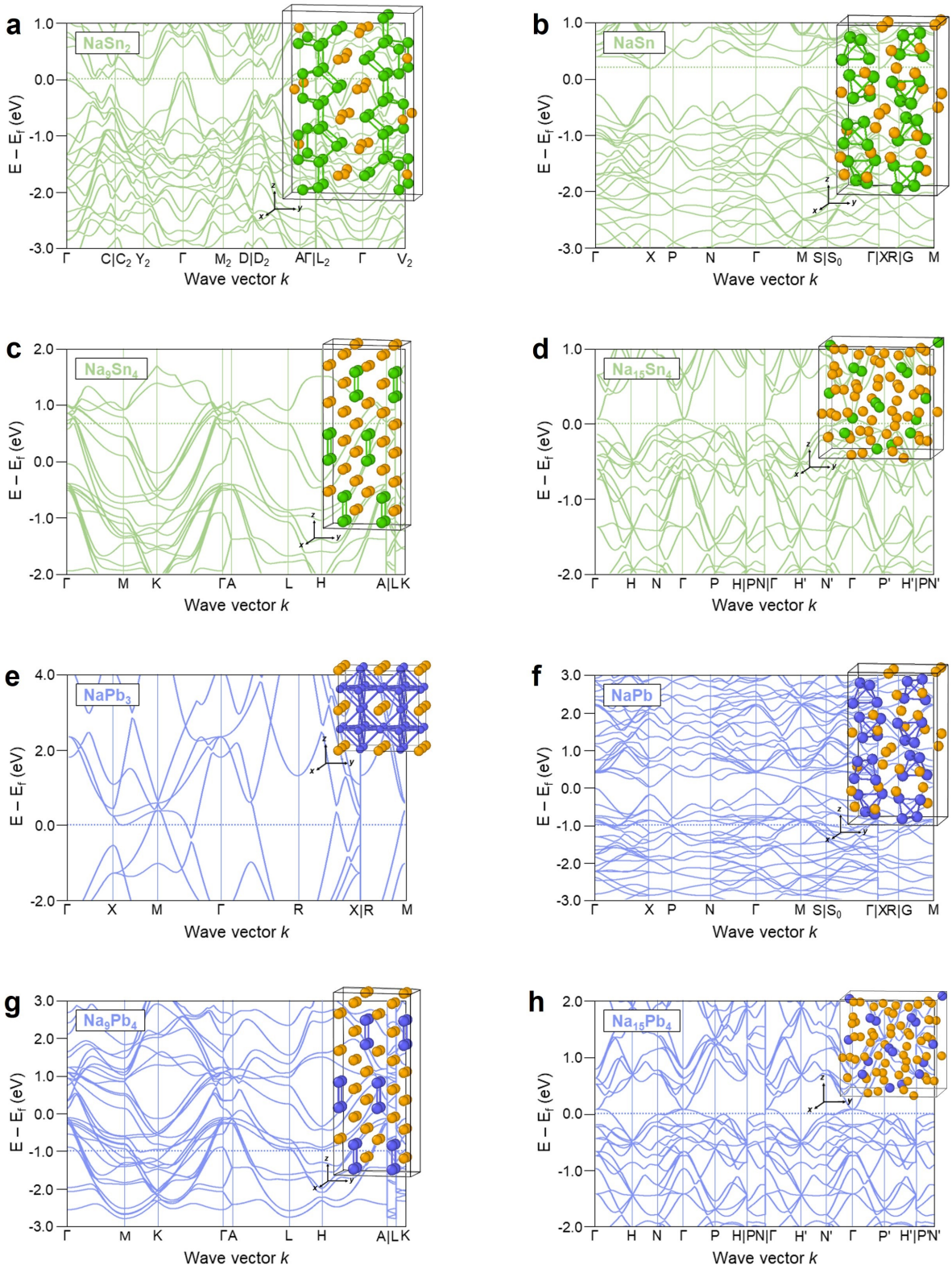

Figure S18. Band structures calculated for the various intermediate phases formed in the (a-d) Na–Sn and (e-h) Na–Pb systems during discharging (or sodiation).

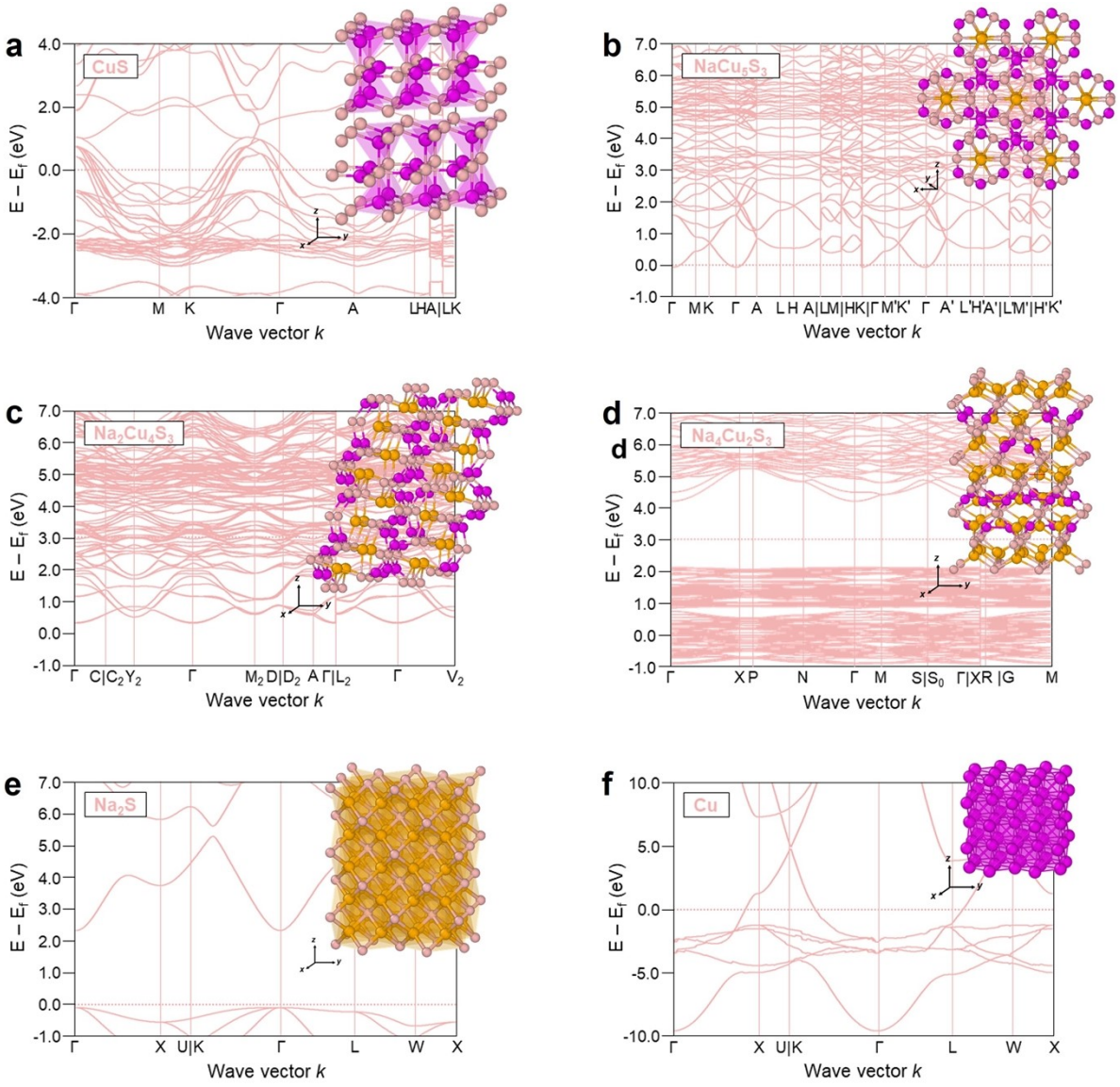

Figure S19. Band structures calculated for the various intermediate phases formed in the Na–CuS system during discharging (or sodiation): (a) CuS, (b) $NaCu_5S_3$, (c) $Na_2Cu_4S_3$, (d) $Na_4Cu_2S_3$, (e) Na_2S, and (f) Cu. The inset images are the corresponding crystal structures.

Table S1. The values of mass, crystal system, density, volume, and volume fraction of each phase involved in the conversion reaction of the Na–CuS system during the first cycle.

Reaction formula	CuS	+	2Na	→	Na_2S	+	Cu
Mass (g)	95.61		45.98		78.05		63.55
Crystal system	Hexagonal		Cubic		Cubic		Cubic
Density (g/cm^3)	4.64		1.05		1.83		8.89
Volume (cm^3)	20.61		43.79		42.65		7.15
Volume fraction	0.32		0.68		0.86		0.14

Table S2. The values of mass, crystal system, density, volume, and volume fraction of each phase involved in the conversion reaction of the Na–CuS system after the fourth cycle.

Reaction formula	$Cu_{1.81}S$	+	2Na	↔	Na_2S	+	1.81Cu
Mass (g)	147.08		45.98		78.05		115.02
Crystal system	Triclinic		Cubic		Cubic		Cubic
Density (g/cm^3)	6.11		1.05		1.83		8.89
Volume (cm^3)	24.07		43.79		42.65		12.94
Volume fraction	0.35		0.65		0.77		0.23

Table S3. The values of the electrical conductivity and volume fraction for each phase involved in the conversion reaction of the Na–CuS system during the first cycle.

Reaction formula	CuS	+	2Na	↔	Na_2S	+	Cu
Parameters	σ_{Cu} (S/m)		V_{Cu}		σ_{Na_2S} (S/m)		V_{Na_2S}
Value	1.51×10^7		0.14		7.83×10^1		0.86

Table S4. The values of the electrical conductivity and volume fraction for each phase involved in the conversion reaction of the Na–CuS system after the fourth cycle.

Reaction formula	$Cu_{1.81}S$	+	2Na	↔	Na_2S	+	1.81Cu
Parameters	σ_{Cu} (S/m)		V_{Cu}		σ_{Na_2S} (S/m)		V_{Na_2S}
Value	1.51×10^7		0.23		7.83×10^1		0.77

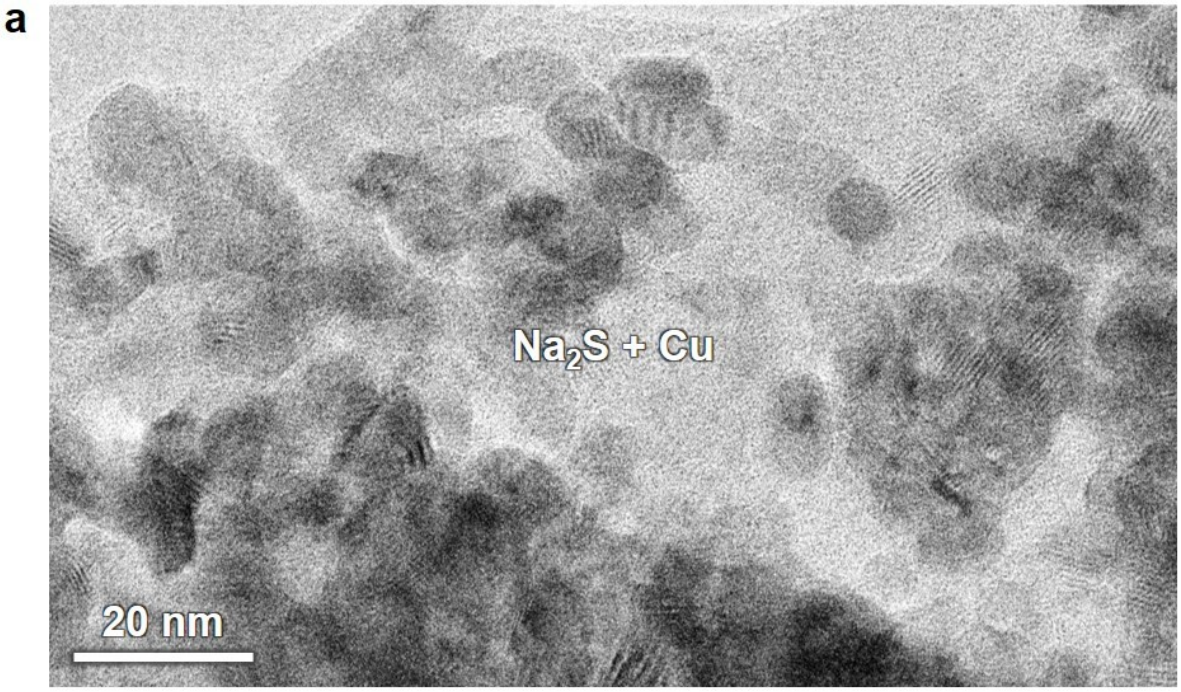

b

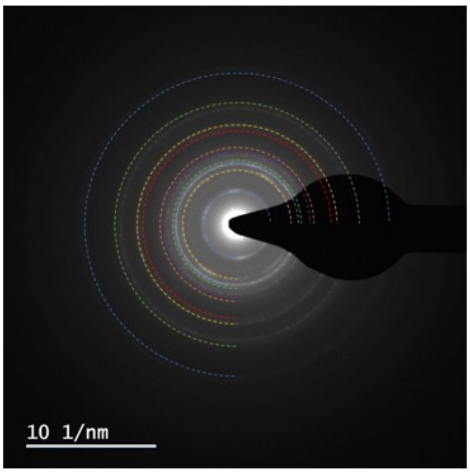

A	B	C	D	E
Order (#)	Measured D-spacing (Å)	Ref. Name	Ref. D-spacing (Å)	Col B / Col D
1	3.835	Na_2S 111	3.79382	101.1%
2	2.393	Na_2S 211	2.32323	103.0%
3	2.135	Cu 111	2.09074	102.1%
4	2.026	Na_2S 221	1.98126	102.3%
5	1.842	Cu 110	1.81063	101.7%
6	1.694	Na_2S 220	1.64277	103.1%
7	1.390	Na_2S 332	1.34132	103.7%
8	1.307	Cu 211	1.28031	102.1%
9	1.070	Cu 221	1.09185	98.0%
10	0.859	Cu 322	0.83077	103.4%

Figure S20. (a) Bright-field image of the Na_2S/Cu composite, showing the uniformly dispersed Cu nanoparticles (dark spots) embedded in the Na_2S matrix (grey background). (b) Selected area diffraction pattern recorded from the Na_2S/Cu composite and corresponding indices.

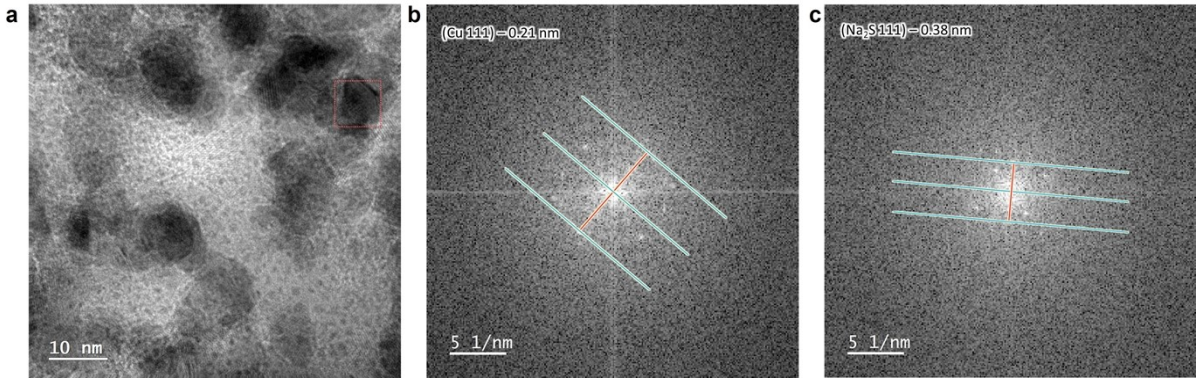

Figure S21. (a) High-resolution transmission electron microscopy image recorded from the Na_2S/Cu composite. The FFT patterns of the dashed red square in (a), showing the presence of (b) Cu and (c) Na_2S phases.

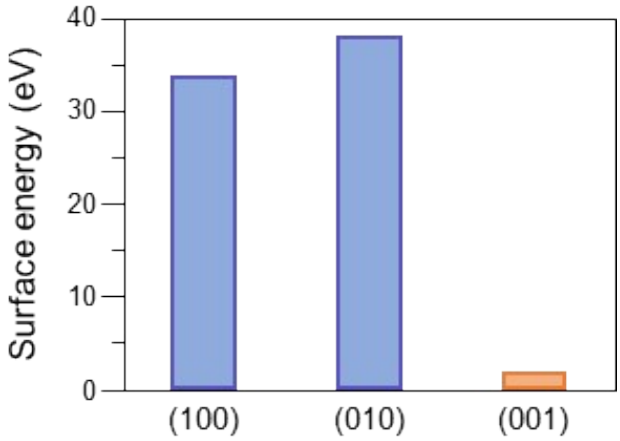

Figure S22. Surface energies of (100), (010), and (001) of hexagonal CuS calculated using DFT calculations.

References

1. P. Giannozzi, S. Baroni, N. Bonini, M. Calandra, R. Car, C. Cavazzoni, D. Ceresoli, G. L. Chiarotti, M. Cococcioni, I. Dabo, A. Dal Corso, S. de Gironcoli, S. Fabris, G. Fratesi, R. Gebauer, U. Gerstmann, C. Gougoussis, A. Kokalj, M. Lazzeri, L. Martin-Samos, N. Marzari, F. Mauri, R. Mazzarello, S. Paolini, A. Pasquarello, L. Paulatto, C. Sbraccia, S. Scandolo, G. Sclauzero, A. P. Seitsonen, A. Smogunov, P. Umari and R. M. Wentzcovitch, *J Phys Condens Matter*, 2009, **21**, 395502.
2. N. Troullier and J. L. Martins, *Phys Rev B Condens Matter*, 1991, **43**, 1993-2006.
3. J. Y. Park, S. J. Kim, J. H. Chang, H. K. Seo, J. Y. Lee and J. M. Yuk, *Nat Commun*, 2018, **9**, 922.
4. G. K. H. Madsen and D. J. Singh, *Computer Physics Communications*, 2006, **175**, 67-71.
5. A. Kundu, M. K. Adak, Y. Kumar and B. Chakraborty, *Inorg Chem*, 2022, **61**, 4995-5009.
6. Y. Wang, Q. Huo, H. Fan, J. Wang and L. Chang, *The Journal of Physical Chemistry C*, 2021, **125**, 11325-11335.